Applied Catalysis B: Environmental 256 (2019) 117858

Contents lists available at ScienceDirect

Applied Catalysis B: Environmental

journal homepage: www.elsevier.com/locate/apcatb

Hierarchical nickel cobalt oxide spinel microspheres catalyze mineralization of humic substances during wet air oxidation at atmospheric pressure

Qi Jing[a], Huan Li[a,b,*]

[a] Shenzhen Engineering Research Laboratory for Sludge and Food Waste Treatment and Resource Recovery, Graduate School at Shenzhen, Tsinghua University, Shenzhen 518055, China

[b] Guangdong Engineering Research Center of Urban Water Cycle and Environment Safety, Graduate School at Shenzhen, Tsinghua University, Shenzhen 518055, China

ARTICLE INFO

Keywords:
Humic substances
Catalytic oxidation
Nickel cobalt oxide
Spinel
Mars-van Krevelen Mechanism

ABSTRACT

Humic substance (HS) is a key pollutant in water supply or wastewater treatment. In this work, hollow microspheres constituted of $NiCo_2O_4$ (NCO) spinel were synthesized and used as the catalyst of catalytic wet air oxidation, aiming to remove HS at atmospheric pressure and low temperature. The results show that NCO had excellent hierarchical architectures with large surface area (66.88 m^2/g), solid-state redox couples, numerous surface oxygen species, and low reduction temperature. When NCO was used to treat HS solution at 90°C, total organic carbon concentration decreased by 93.4% after 24 h. NCO itself had the ability to mineralize the HS adsorbed on the surface, and dissolved oxygen can fill oxygen vacancies and recover NCO to its original state. Hydroxyl radicals also assisted the HS degradation. These findings provide some insight into the HS degradation process and promise an inexpensive and easy way to clean HS-rich water or wastewater.

1. Introduction

Humic substance (HS) is a type of natural organic polyelectrolyte [1,2] that usually exists in natural water bodies, soil, compost, municipal sewage, and landfill leachate [3]. HS can be divided into three categories, humic acid (HA), fulvic acid (FA), and humin (HU), according to their solubility in alkaline or acidic solution [4]. HS plays an important role in maintaining soil function [5], but it becomes a negative factor during water or wastewater treatment. HS brings unpleasant color and odor to water, and it is also the key precursor of disinfection byproducts during chlorination of drinking water [1,6]. HS contains a large number of oxygencontaining functional groups, such as carboxyl groups, phenolic hydroxyl groups, alcoholic hydroxyl groups, methoxy groups, and carbonyl groups [7]. These functional groups have the abilities of ion exchanging, weak acidity, adsorption, complexation, redox, etc. [8], and accordingly, HS interacts in various ways with other compounds. These interactions can reduce the biochemical reactivity of some pollutants and degrade their treatment effects [1]. For example, HS can inhibit sludge hydrolysis [9], adsorb toxic organic compounds and heavy metals ions [10,11], and consequently, hinder organic removal during anaerobic digestion. In addition, HS in digested effluent increases the electronegativity and hydrophilicity of sludge particles, and thus reduces the flocculation ability of these particles [12]. Therefore, it is of considerable importance to develop methods of HS degradation or removal from water and wastewater.

However, it is difficult to remove it through common biological treatment processes, because HS is a type of organic mixture that has complex molecular structures, and its main parts, such as aliphatic chains, aromatic hydrocarbons and polysaccharides, have poor biodegradability [13]. Conventional physicochemical technologies, including flocculation [14], filtration [15], and adsorption [16], require excessive consumption of chemicals and energy. Advanced oxidation processes (AOPs) are the methods that can mineralize HS based on free radical oxidation, for example, ozone oxidation [17], fenton/efenton [18], photocatalysis [19], peroxymonosulfate oxidation [20,21], and photochemical oxidation [22]. Cortez et al. [17] treated mature landfill leachate with O_3 and H_2O_2, and 53% of total organic carbon (TOC) and 63% of chemical oxygen demand (COD) were removed at doses of 112 mg/L O_3 and 600 mg/L H_2O_2. Čehovin et al. [18] decomposed HS in drinking water at 0.3 and 1.8 J/cm^2 ultraviolet radiation, 2–14 mg/L O_3 and 1–12 mg/L H_2O_2, and the TOC removal rate reached 25.7%. Typically, AOPs are considered to be economic, green, and widely accepted for the efficient degradation of organic pollutants in wastewater. However, regarding wastewater rich in HSs, such as landfill leachate, the effect will be different. Photocatalysis may be not an appropriate choice owing to the poor light transmission of that kind of wastewater. Moreover, HS is generally entrapped with other components, and thus the dose of strong oxidizing agents like O_3, H_2O_2, or peroxymonosulfate

* Corresponding author at: Building of Energy and Environment, Tsinghua Campus, University Town, Room 2113 Shenzhen, China.
E-mail address: li.huan@sz.tsinghua.edu.cn (H. Li).

https://doi.org/10.1016/j.apcatb.2019.117858
Received 13 March 2019; Received in revised form 27 May 2019; Accepted 9 June 2019
Available online 15 June 2019
0926-3373/

will be quite high. In contrast, molecular oxygen (air or pure oxygen) is cheaper and can be also used as the oxidant in wet air oxidation (WAO) [23]. However, WAO operations require high temperature (125–320 °C) and high pressure (0.5–20 MPa). Catalytic wet air oxidation (CWAO), though, not only promotes the degradation of refractory organic pollutants, but also greatly reduces the reaction conditions, thereby reducing capital and operational costs.

Nowadays, many studies have been made on CWAO treatment at pilot scales, mostly performed in trickle-bed reactors at oxygen partial pressures of 0.1–3.0 MPa and temperatures of 100 °C – 280 °C using catalysts like Pt, Al_2O_3, CuO, carbon materials [23–30]. Delmas et al. [31] degraded 4-hydroxybenzoic acid over activated carbon in a fixed bed reactor, and more than 90% of the 4-hydroxybenzoic acid was removed within 1500 min at an oxygen partial pressure of 0.2 MPa and temperature of 140 °C. Lopes et al. [26,32] studied the Computational fluid dynamics of trickle-bed reactor modelling in the CWAO of phenols using a commercial catalyst CuO-MnO_x at an oxygen partial pressure of 3 MPa and temperature of 160 °C – 200 °C. Wu et al. [33] treated phenols using copper/activated carbon catalyst at an oxygen partial pressure of 1.0–3.0 MPa and temperature of 40–60 °C and found that the performance of the reactor depended largely on the gas-to-liquid mass-transfer process. Despite the obtained performance, it is always a desirable trend to decrease the energy and expenditure of waste or wastewater treatment. Thus, some catalysts have been developed toward achieving milder conditions for CWAO. Sun et al. [34,35] used 2.72 g/L Mo-*Zn*-Al-O as the catalyst during CWAO of 0.085 g/L cationic red GTL at ambient pressure, and the removal efficiencies of color and TOC reached 90.9% and 65.8% in 1 h, respectively. Li et al. [36] used 2.53 g/L polyoxometalate in CWAO of 0.068 g/L phenol at ambient pressure, and 93.0% of the TOC was removed in 90 min.

However, HS is more difficult to degrade, and the reaction conditions required by CWAO are still harsh. Oulego et al. [37] carried out CWAO of landfill leachate at an oxygen partial pressure 6.0 MPa and temperature of 180 °C, and the mineralization degrees reached 72%, 54%, and 51% for the extracted humic fraction of landfill leachate, commercial humic acid, and stabilized landfill leachate, respectively, after 480 min. Some works used other oxidants, e.g., hydrogen peroxide [38], potassium persulfate [39], and 2,4,6-trichlorophenol/$NaNO_2$ [40] to enhance CWAO of HS wastewater, and their COD removal rates reached 78% (22 min), 77.8% (4 h), and 19.3% (4 h), respectively. To avoid the consumption of these chemicals and the generation of toxic by-products [1], new catalysts are still the research focus regarding CWAO of HS wastewater under mild conditions.

Nickel cobalt oxide ($NiCo_2O_4$, abbreviated NCO) with spinel structure is a type of promising functional material [41–44] that has many intriguing advantages, such as good redox ability, high electronic conductivity, low cost, and environmental friendliness [42]. NCO has been applied to lithium-ion batteries, supercapacitors, electrocatalysts, and AOPs [42,43]. Tian et al. [45] and Zhang et al. [46] studied the catalytic performance of NCO for peroxymonosulfate activation in organic pollutant degradation, and Liu et al. [47] verified that NCO displayed superior catalytic activity for Congo red under microwave irradiation. Furthermore, the spinel structure facilitates the absorption of oxygen on the surface, and the oxygen species (both lattice oxygen and non-lattice oxygen) of the spinel are active oxygen species that play a critical role in oxidation reactions [21,22,48,49]. The wide application of NCO in the oxygen reduction reaction (ORR) [44,50] also confirms its catalytic performance in converting O_2. These abilities could make great contributions to the mass transfer of O_2 and to oxidation of HS in water. Hence, NCO could have great potential in CWAO of refractory organics under mild conditions, but several of its characteristics related to CWAO and its usage in CWAO, to the best of our knowledge, have not been previously studied.

In this study, urchin-like $NiCo_2O_4$ hollow microspheres were synthesized for the mineralization of HS during CWAO under mild conditions, i.e., atmospheric pressure and temperature lower than 90 °C. Catalyst characterization, kinetics experiments, analyses of intermediates, and the detection of hydroxyl radicals were carried out to investigate the mechanism of NCO catalytic oxidation. In particular, the role of NCO in CWAO was first analyzed by its component elements' valence-state changes, free radicals in the reaction system, and so on, and the evolution of the molecular weight distribution of HS solution during CWAO was investigated. The results are expected to provide some insight into the effect of NCO during CWAO and help innovate a new method for HS mineralization that is both easy and inexpensive.

2. Materials and methods

2.1. HS and other reagents

The reagents and solvents used in this study were of analytical reagent grade, and were not further purified. A commercial HS (sodium humate) was supplied by Aldrich Chemistry, USA, and its Fourier-transform infrared-spectroscopy (FTIR) profile is shown in Fig. S1 (see Supplemental Information). HS was dissolved in deionized water at a concentration of 25 g/L, and the resulting suspension was then centrifuged at 5800 *g* for 10 min to collect the supernatant and remove the residuals. The supernatant was adjusted to different pH values and diluted to different concentrations as needed, and then used for CWAO experiments.

2.2. Synthesis and characterization of the catalyst

The urchinlike NCO hollow microspheres were synthesized by a solvothermal method followed by calcination according to the literature [43]. Typically, 0.08-mol $Co(NO_3)_2{\cdot}6H_2O$, 0.04 mol Ni $(NO_3)_2{\cdot}6H_2O$ and 4.80-mol urea were dissolved in a mixture of isopropanol (IPA, 1200 ml) and water (240 ml). The resulting mixture was stirred thoroughly to ensure uniform mixing of all the ingredients. The mixture was transferred into Teflon™-lined stainless-steel vessels (purchased from Anhui Kemi Machinery Technology Co., Ltd), which were then heated at 120 °C for a period of 12 h in an electric oven. Next, the vessels were cooled naturally to room temperature, and the mixture in the autoclaves was then centrifuged to collect the precipitate. The precipitate was washed using deionized water and ethanol several times and then dried at 105 °C overnight. All of the synthesized products were calcined at 350 °C in air for 2 h at a ramping rate of 1 °C/min. The final amount of synthesized $NiCo_2O_4$ was approximately 15 g in a yield of 80.8%.

The morphological and chemical composition of the synthesized NCO were studied by scanning electron microscopy (SEM, ZEISS SUPRA 55, Germany). X-ray diffraction (XRD, RINT2000 V/PC, Bruker DS, Germany) was used to obtain the crystallographic information and chemical states of the synthesized NCO. X-ray photoelectron spectra (XPS) were measured by using an ESCALAB-MKII spectrometer (UK) with Al Ka radiation (1486.6 eV), and the raw spectra were curve-fitted by non-linear least squares fittings with a Gauss-Lorentz ratio (80:20) through the XPS PEAK41 software. Nitrogen sorption measurement was conducted at 77 K using an analyzer (ASAP-2020, Micrometrics, U.S.A.). Prior to analysis, the samples were degassed under vacuum at 120 °C for 24 h. The specific surface area (SSA) was calculated using the multipoint Brunauer-Emmett-Teller (BET) method, and the pore size distribution (PSD) and pore volume data were calculated from the desorption branch based on the Barrett-Joyner-Halenda (BJH) equation [43]. Temperature-programmed reduction by H_2 (H_2-TPR) was performed using a Micromeritics AutoChem II 2920 with 10% H_2 in argon at a total flow rate of 25 ml/min. The temperature range studied extended from room temperature to 700 °C at a heating rate of 10 °C /min. Prior to the reduction, the samples were pretreated at 105 °C for 1 h air to be dried throughly and then cooled down to room temperature. Zeta potential change depending on pH was determined by Nano/Zetasizer (ZS90, Malvern Instruments Ltd.) for the calculation of isoelectric point

(pH_{iep}).

2.3. CWAO of HS

CWAO was carried out in anaerobic and aeration modes. All experiments were performed in triplicate. Some reaction parameters, such as temperature and pH, differed depending on the purpose of experiments, but the basic experimental procedure remained the same.

Anaerobic mode was used to explore the interaction between NCO and the HS without external oxygen. Experiments were carried out in air-proofed bottles, and 10 mL of HS solution and 50 mg of NCO were added to each bottle. The bottles were first blown with nitrogen in advance to eliminate the initial air in the head space, and were then placed in a water bath for reactions. After pre-determined time intervals, the bottles were removed from the water bath in sequence, and then quickly placed in an ice-water bath to stop the reactions inside the bottles. After cooling, the mixtures in the bottles were centrifuged at 5800 *g* for 80 min. The supernatant was collected and then filtered with a 0.45-μm aqueous membrane. The filtrate was used for further analysis. The used NCO precipitation in the centrifuge tubes was washed using ultrapure water to remove the residual solution, while the filtration residual of NCO was freeze-dried to ensure that the valences of the elements in NCO were not affected by thermal drying.

Experiments in aeration mode were carried out in a series of 2-L glass reactors, each equipped with a reflux condenser, magnetic stir-heater, aeration device, and sampling valve. In a typical run, a group of reactors were used, and a 1-L HS solution and 5 g of NCO were added to each reactor. These reactors were heated from room temperature to a certain reaction temperature. Next, magnetic stirring was started, and oxygen was immediately bubbled into the solutions continuously at a rate of 250 mL/min to ensure that there was excess oxygen in the reaction. For convenient discussion, this moment was defined as the "zero time" of the run. After 3, 6, 12, 24, and 48 h, solution samples containing used NCO were collected from different reactors. The samples were treated with the same methods as described in anaerobic mode.

2.4. Other analytical methods

TOC was determined by a TOC IR analyzer (TOC-L_{CSH}, Shimadzu, Japan), and COD was determined according to standard methods (MEP, 2002) [51]. Fourier transform infrared (FTIR) spectra of HS was obtained using a Shimadzu FTIR-8400S spectrophotometer over a 4000–400 cm^{-1} range. Electron spin resonance (ESR) signal of radicals was obtained on a Bruker ESR 300 E spectrometer with an irradiation source of Quanta-Ray pulsed Nd:YAG laser system. The chemical agents for spin-trapping ·OH was 5,5-dimethyl-1-pyrroline-*N*-oxide (DMPO). For all the samples, the same quartz capillary tube was used to minimize experimental errors.

An matrix-assisted laser desorption/ ionization time of flight mass spectrometry (ABI 4800 MALDI TOF/TOF, Applied Biosystems, U.S.A.) with a 3–7 ns ND:YAG laser (355 nm) with a maximum intensity of 5000 (arbitrary units) was used to detect molecular size change of HS during CWAO. MALDI TOF MS is an innovative tool to detect the absolute molecular weight (MW) rather than the apparent MW detected by chromatography and ultrafiltration [52]. It has the advantage of forming singly charged ions over electron spray ionization (ESI), and its operation is much more convenient than ESI (electrospray ionization)-TOF-MS [52]. A reflectron and a positive modes were used. The intermediates test was carried out using the solutions from the aeration reactors at 90 °C and initial pH of 10. To get better spectrum, these solutions were concentrated about 20 times by mixing with acetonitrile at a volume ratio of 7:3 followed by nitrogen sweeping. Each sample was first mixed with acetonitrile according to volume ratio of 7:3, then mixed with the same amount of matrix solution containing 10 mg/mL DHBA, and spotted onto a 384-well stainless-steel MALDI target plate. Intermediates were detected by GC-MS (GC-MS-7980B-5977, Agilent, American) referring to the previous report [53]. Volatile fatty acids were measured using a gas chromatograph (GC-2014, Shimadzu, Japan) equipped with a capillary column (Inertcap wax 30 m × 0.25 mm × 0.25 μm) and a flame ionization detector.

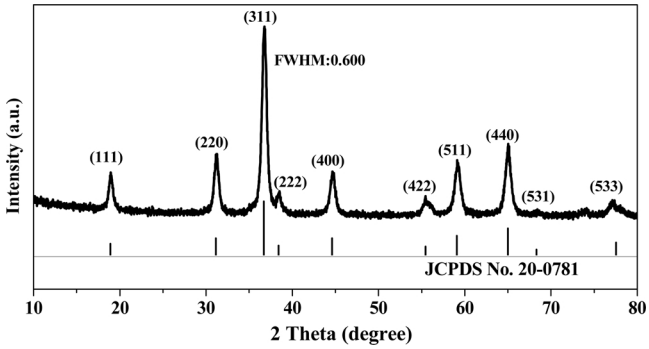

Fig. 1. XRD pattern of the synthesized NCO.

3. Results and discussion

3.1. Catalyst characterization

The XRD pattern of NCO was recorded and is shown in Fig. 1; the resultant diffraction peaks identify well with the standard patterns of cubic spinel NCO (JCPDS Card No. 20-0781) [42,43]. There are no peaks of impurities observed from this pattern, certifying that the spinel NCO was synthesized successfully. According to the Debye-Scherrer formula [Eq. (1)], the average NCO crystallite size was calculated to be approximately 14 nm based on the strongest peaks [the (311) peak]:

$$D = k\lambda/(\beta\cdot\cos\theta), \quad (1)$$

where D is the average crystallite size, k is the Scherrer constant (0.89), λ is the wavelength of X-ray radiation (1.5406 Å), β is the full width at half maximum (FWHM) of the diffracted peak, and θ is the Bragg angle of diffraction. According to the calculation performed in Jade 5.0, the FWHM of the (311) peak is 0.600.

The morphology of the NCO is shown in Fig. 2. Figs. 2A–C show that the NCO particles have a microspherical structure, with the microspheres having diameters of approximately 3–5 μm, and they resemble hollow urchin shells. Fig. 2D shows the three-dimensional hierarchical architectures of NCO, which is self-assembled from these low-dimensional nanostructured building blocks and secondary architectures such as nanorods radially grown from a common center. This kind of unique morphology would make a significant contribution to catalytic oxidation performance of NCO, as it can offer a high specific surface area, more active sites for reaction, short diffusion paths for ions or electrons, high-energy adsorption capacity, and efficient channels for mass transport [43,47].

Areas 1 and 2 in the EDS spectrum of NCO (Fig. 3A) are plotted in Figs. 3B and 3C, respectively. The calculated atomic ratio of Ni/Co/O was 1:2.06:5.44, while the ratio should be 1:2:4 for the stoichiometric spinel NCO. The excessive oxygen species might be sourced from surface oxygen of the NCO, including oxygen in OH^- and absorbed oxygen (oxygen ions in low-coordination sites at the surface), and multiplicity of physisorbed and chemisorbed water at or within the surface [21,42,54–56]. These oxygen species are considered to play a significant role in the performance of catalyst [23].

Nitrogen adsorption measurements were conducted to investigate the surface structure of NCO, and the nitrogen adsorption isotherms are shown in Fig. 4A. The isotherms exhibit typical Langmuir type-IV curves with an obvious hysteresis loop in the P/P_0 range 0.7–1.0, which is the significant feature of mesoporous materials. The pore-volume plots in Fig. 4B and the pore-size distribution plots in Fig. 4C were

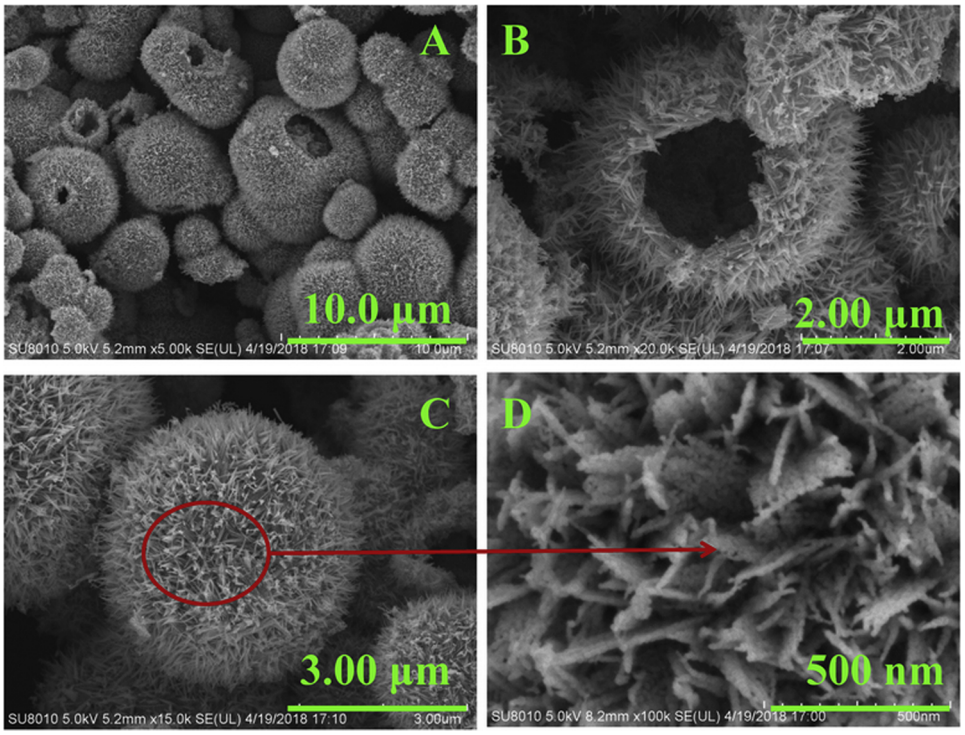

Fig. 2. SEM images of the NCO with the amplification times of 5000 (A), 20,000 (B), 15,000 (C), 100,000 (D).

obtained using the Barret-Joyner-Halenda (BJH) model. The pore-size distribution was centered at 6.94 nm and the mesoporous volume was approximately 0.35 cm^3/g, indicating the superior mesoporous nanostructures of NCO. In contrast, the SSA, total pore volume, and average pore diameter calculated using the Brunauer-Emmet-Teller (BET) equation were 66.88 m^2/g, 0.4108 cm^3/g, and 24.57 nm, respectively. These differences can be attributed to the existence of larger mesopores (20–50 nm) [43]. Combined with the results of SEM, the hierarchical mesoporous nanostructures of NCO can be clearly determined. It is well known that mesoporous structures are critical to the performance of catalysts as they can provide intriguing physical and chemical properties, including high SSA, sufficient active sites distributed at the exterior surface (but also within the large interior surface of the catalysts), excellent accessibility to active sites for molecules in the bulk, and enhanced mass transport and diffusion [57,58].

Valence states of constituent elements of NCO were detected using

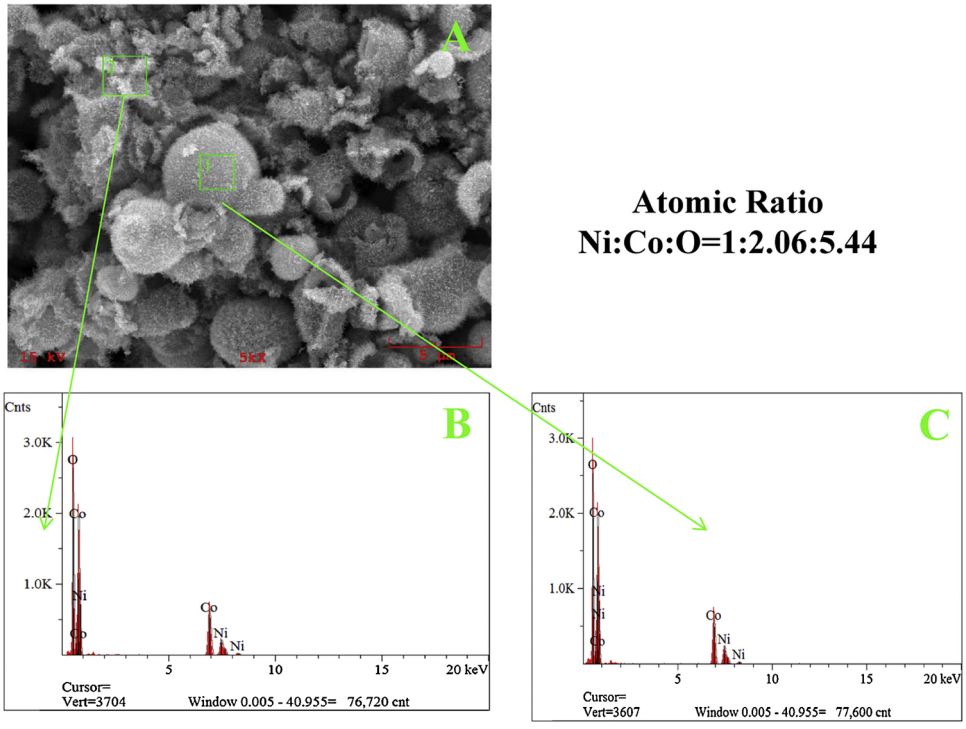

Fig. 3. SEM images of the NCO with the amplification time of 5000 (A), and EDS analysis report of area 1 (B) and area 2 (C).

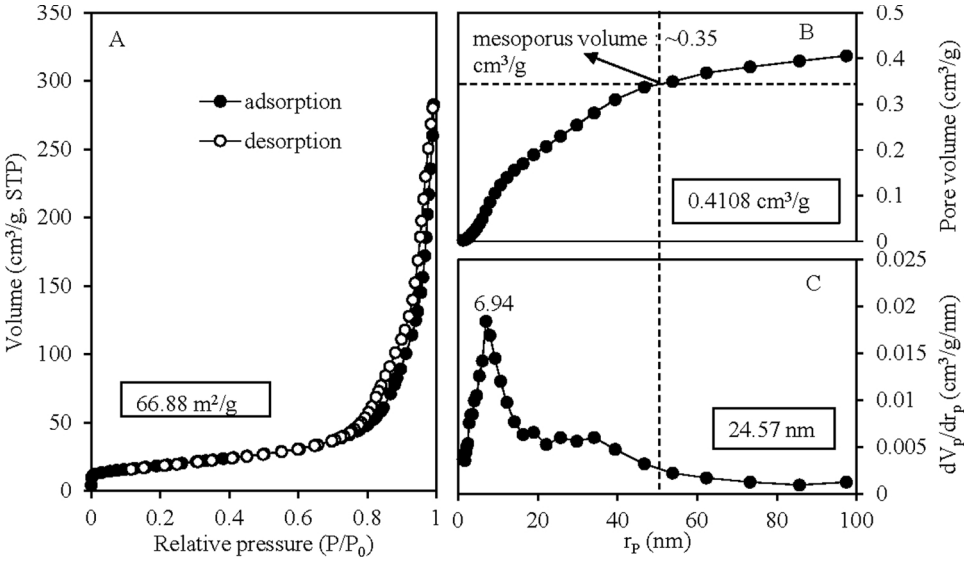

Fig. 4. Nitrogen adsorption-desorption isotherm plot (A), pore volume plot (B) and pore size distribution plot (C) of the NCO catalyst; the pore size distribution was centered at 6.94 nm (C) and the mesoporous volume was about 0.35 cm^3/g (B) according to BJH model; and the SSA, total pore volume and average pore diameter were 66.88 m^2/g (A), 0.4108 cm^3/g (B) and 24.57 nm (C) according to BET model.

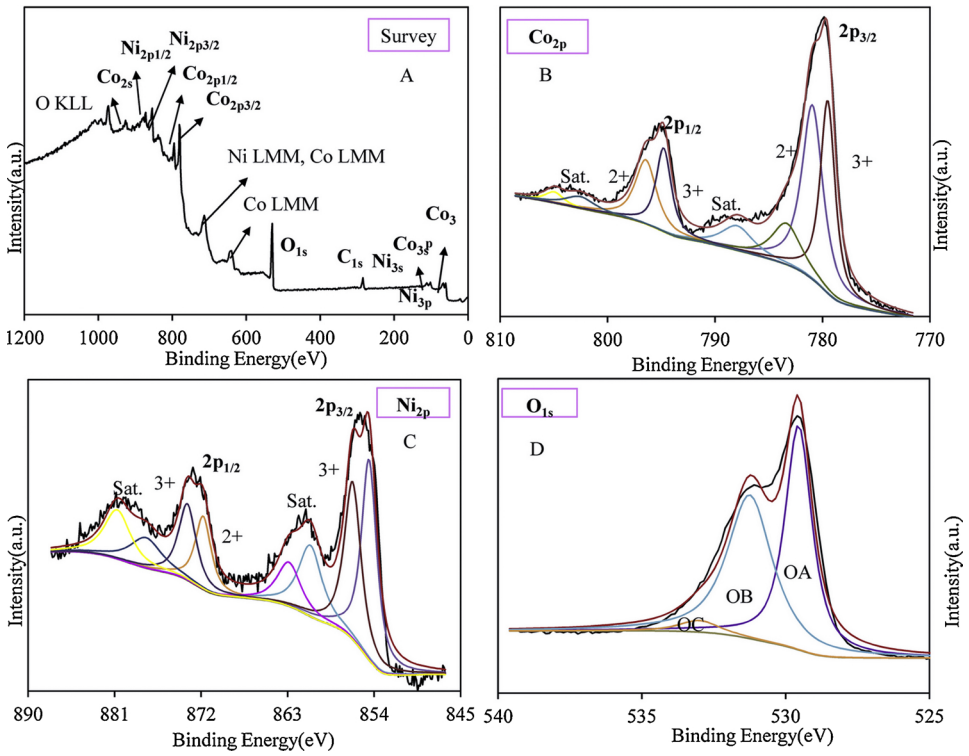

Fig. 5. XPS profiles of the NCO catalyst: survey scan (A), O_{1s} core level (B). Ni_{2p} core level (C) and Co_{2p} core level (D).

XPS. The typical signals of O_{1s}, Co_{2p}, and Ni_{2p} core levels were obviously observed (Fig. 5A). The Ni_{2p} and Co_{2p} spectra (Figs. 5C and 5B) both consist of two spin-orbit doublets and two shakeup satellites (denoted "Sat."), and the two spin-orbit doublets of these two spectra are ascribed to Ni^{2+} and Ni^{3+} (or Co^{3+} and Co^{2+}) [42]. These results show that the surface of NCO has a composition containing Co^{2+}, Co^{3+}, Ni^{2+}, and Ni^{3+} species. The O_{1s} spectra (Fig. 5D) exhibit three oxygen contributions. The fitting peak at 529.5 eV (denoted OA) is derived from typical metal-oxygen bonds. The peaks located at 531.8 eV, denoted OB, should be attributed to chemisorbed oxygen or a hydroxyl-like group (oxygen ions in low-coordination sites at the surface). The peaks at 533 eV, denoted OC, are attributed to physisorbed/chemisorbed water at and within the surface [21,23,42,54–56]. Previous studies have shown that OA and OB are active and essential oxygen species [21,56,59] for participation in oxygen delivery, and they can take an active part in catalytic oxidation processes. The mobility of OB is considered to be higher than that of OA [23,60]. Besides, the OB species have the ability of reacting with organic substance directly [61,62] or facilitating electron transfer to produce radicals [61,63]. OA and OB are considered to be transformed to each other according to the Mars–van Krevelen (MVK) mechanism. Typically, OB species are consumed first, and then OA species are released to the surface and converted to OB species under anoxic condition. OB species oxidize the substrate while forming several oxygen vacancies, and the catalyst will be re-oxidized to its initial state when O_2 fills the oxygen vacancies [64,65].

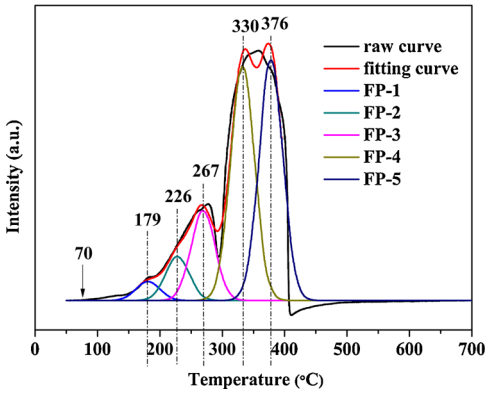

Fig. 6. H_2-Temperature-programmed reduction profiles of the NCO catalyst.

The reduction behavior of NCO was investigated using H_2-TPR. The H_2-TPR results and that of their peak-differentiating analysis are shown in Fig. 6. There were five well-defined reduction fitting peaks in the TPR profile of NCO (abbreviated FP-*x*, where *x* is 1, 2, 3, 4, or 5). The onset reduction temperature appeared at approximately 70 °C, which can be attributed to the reduction of chemisorbed oxygen. FP-1 at 179 °C is attributed to surface oxygen species [66], particularly to chemisorbed oxygen. Thus, it can be confirmed that NCO has good oxygen capacity, which can correspond to the conclusion from XPS (shown in Fig. 4). FP-2 at 226 °C and FP-3 at 267 °C are highly overlapped, and they are attributed to the reduction of Ni^{3+} to Ni^{2+} and Co^{3+} to Co^{2+}, separately [67], indicating the synergistic effect of Ni and Co. FP-4 at 330 °C and FP-5 at 376 °C also evidence a similar situation, and they are attributed to the reduction of Ni^{2+} to Ni^0 and Co^{2+} to Co^0 [67]. Previous studies reported several H_2-TPR profiles of NCO. Wang et al. [68] synthesized NCO according to the hard template method and found that the reduction peaks of H_2-TPR appeared at 355 °C and 682 °C. Zhang et al. [69] studied the H_2-TPR of NCO synthesized by the sol-gel method and found reduction peaks at 386 °C and 547 °C. Wang et al. [67] tested the H_2-TPR profiles of two kinds of NCO synthesized with different methods. The well-defined peaks of NCO synthesized using co-precipitation appeared at 354 °C, while those of NCO synthesized using the hard template method appeared at 253 °C and 323 °C with much better catalytic reduction performance of NO_x than the former one. Compared to previous studies, the reduction peaks of NCO in this work appeared at lower temperatures, implying better catalytic performance [67]. Moreover, the existence of chemisorbed oxygen presents the ability to combine O_2, which would decrease the oxygen partial pressure required by CWAO.

3.2. Catalytic performance of NCO in oxidative degradation of HS

The degradation of HS was investigated at different conditions of CWAO, including temperature, initial pH, and oxygen supply. Both temperature and pH could affect the activity of NCO by affecting the absorbed energy of active species of NCO or its surface charge. The effect of oxygen supply was investigated using two modes, anaerobic and aeration, at 250 mL/min. The former mode was used to explore the interaction between NCO and HS, while the latter was used to investigate the catalytic performance of NCO in CWAO of HS.

3.2.1. Effect of temperature on reaction between NCO and HS

Kinetic tests of NCO and HS were carried out in anaerobic mode at 25 °C, 60 °C, and 90 °C and an initial pH of 10. In the group with an initial TOC (TOC_0) of 107.8 mg/L (Fig. 7A1 and B1), the removal rates of TOC reached 48.3%, 53.5%, and 94.8%, respectively, at the three temperatures after 48 h, while they were 48.7%, 58.5%, and 91.9%, respectively, for COD removal. The removal rates of TOC and COD at 60 °C exhibited a slight improvement compared to those at 25 °C, but

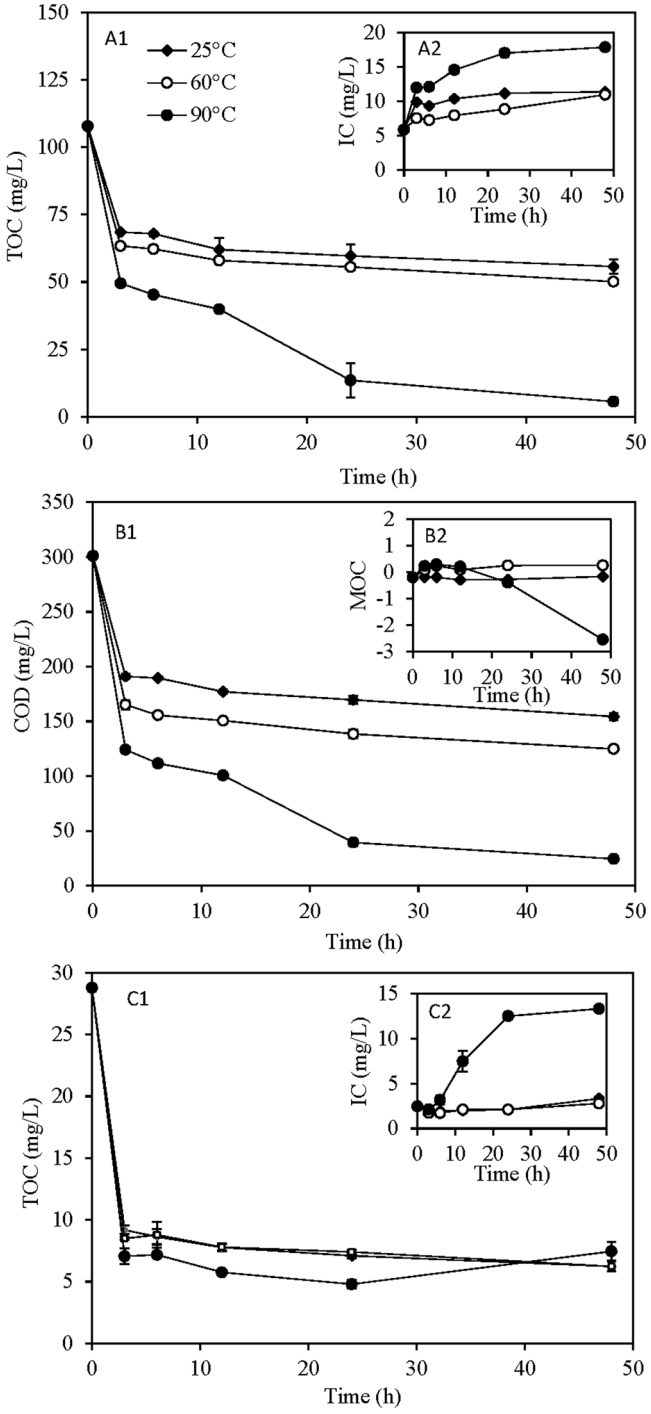

Fig. 7. HS removal with the assistance of NCO in anaerobic mode (at pH 10 and without external oxygen supply) at 25, 60, 90 °C and initial pH of 10 (A1, A2, B1 and B2 were plotted at TOC_0 of 107.8 mg/L; C1 and C2 were plotted at TOC_0 of 28.8 mg/L).

the improvement was greater when the reaction temperature increased to 90 °C. Obviously, the oxidation performance of NCO was strongest at 90 °C because of enhanced transmission and reaction between NCO and organics according to the Arrhenius law.

In the group with a TOC_0 of 28.8 mg/L (Fig. 7C1), TOC removal rates reached 78.3%, 78.4%, and 71.4% after 48 h, respectively, at 25, 60 and 90 °C, and they were basically equal expect for a decrease at 90 °C. Compared to the two batches of experiments, it was deduced that the HS was first absorbed on NCO due to the electrostatic interaction mechanism [70], and then oxidized by NCO to small organic molecules.

Some of the micro-molecules could be desorbed from the surface of NCO, and the rate of desorption from the NCO surface to the bulk environment should be higher than the rate of adsorption from the bulk environment to the NCO surface at the last stage at 90 °C. In contrast, in the group with a TOC_0 of 107.8 mg/L, the HS in bulk solution was always sufficient throughout the entire reaction process, and the rate of adsorption was always higher than that of desorption. Thus, the amount of TOC decreased all the time.

The increase of inorganic carbon (IC) concentration was also recorded over time (Fig. 7A2 and C2), verifying the mineralization of the HS owing to NCO. It should be noted that the IC values presented were smaller than the actual values, because it was detected that some IC was absorbed on NCO surface. The mean oxidation state of carbon (MOC) was also calculated (Fig. 7B2) according to the equation $(4 - 1.5 \times COD/TOC)$ [37,71,72]. The MOC value must always lie in the range [-4, +4], and some aqueous organics, e.g., aliphatic short-chain alcohols, acetaldehyde, etc., have a negative MOC, and short-chain organic acids have a positive MOC [37,71]. During the reaction processes, the change of MOC value was negligible at 25 °C and 60 °C, while the value first increased to 0.30 and then decreased to −2.54 at 90 °C after 48 h. These results confirm the effect of temperature on the reaction. At 90 °C, the HS adsorbed on NCO surface was oxidized to generate intermediates in the low oxidation state with positive MOC values, and then they were desorbed from NCO surface. The final decrease of MOC should be attributed to the COD caused by the reduced nitrogen compound [71].

3.2.2. Effect of pH on reaction between NCO and HS

Anaerobic experiments of HS removal with a TOC_0 of 107.8 mg/L were also conducted for 3 h at different initial pH values (Fig. 8). The effects of pH on the removal of TOC were very limited, and the rates reached 35%, 45%, and 55% at 25 °C, 60 °C, and 90 °C, respectively. In contrast, the removal rates of COD were different, which reached approximately 36.5% at initial pH values of 7, 8, and 10, while reaching 46.5% at pH 12 at 25 °C. The same tendency manifested at 60 °C and 90 °C, and the highest COD removal rate (71.9%) occurred at pH 12 at 90 °C. This implies a variation of MOC of the solutes with the same TOC concentrations. Actually, the MOC of the initial HS was approximately −0.189, and after 3 h of reactions at 90 °C the MOC of intermediates became positive at pH 10, 11, and 12.

These results strongly indicate that OH^- served an essential purpose during the interaction between the HS and NCO, and to some degree, might improve the activity of NCO to decompose HS. To explore the role of OH-, a zeta-potential test was carried out (Fig. S2), the results of which show that the pH_{iep} of NCO was 7.9. As pH increased, the zeta potential of NCO became more negative, which could be explained by the strong combination of OH- and NCO due to ≡Ni and ≡Co ions serving as the active Lewis sites. Thus, strong oxidizing species might be formed, such as ≡Ni−OH or ≡Co−OH, which can oxidize HS. In addition to oxidation, the adsorption of HS on metal oxide is also pH-dependent [70,73]. Metal oxides tend to be protonated and easy to combine with negatively charged HS due to their carboxylic and phenolic groups [61,64]; when OH- concentration increases, the deionization of the surface of the metal oxide would be inhibited, thereby reducing the adsorption of the HS on the metal oxide. Furthermore, the adsorption follows the electrostatic interaction, which becomes weak as temperature increases. Therefore, the increase of pH and temperature should be adverse to HS electrostatic adsorption on NCO, but favor the oxidation of the HS. At low temperature and pH, the electrostatic interaction played a leading role as the oxidation activity of NCO was weak. The HS and its intermediates had more electrons, and the MOC of their solution remained negative. When temperature and pH increased, more oxidative species decomposed more organics, resulting in a positive MOC in solution.

3.2.3. Effect of oxygen supply on CWAO of HS using NCO as catalyst

In aeration experiments, O_2 was bubbled to the reactors continuously, and the performance was compared with that in anaerobic mode (Fig. 9). For the group with a TOC_0 of 107.8 mg/L, TOC removal reached 93.4% in anaerobic mode and 48.3% with O_2 supply. It seemed that O_2 bubbles decreased the organic removal rate. However, the MOC of the solution with O_2 supply kept increasing to positive, indicating that O_2 promoted oxidation of the HS on the NCO surface and released more short-chain organic acids to the solution. Small molecular carboxylic acids were considered as refractory species for CWAO [37,38]. For the group with a TOC_0 of 28.8 mg/L, TOC removal rates reached 74.1% in anaerobic mode and 95.5% in aeration mode at 90 °C, indicating the promotion of HS degradation via O_2 supply.

In the two groups with different TOC_0 values, oxygen supply resulted in different effects, possibly owing to the variation of the NCO structure and intermediate concentration. A high aeration intensity was adopted in this study to keep excessive oxygen in the reactors, but oxygen bubbling and manganese stirring could break and collapse the hierarchical structure of the NCO mechanically after a period of reaction in aeration mode (Fig. S3). In contrast, NCO retained structural integrity in anaerobic mode. Nevertheless, the XRD pattern (Fig. S4)

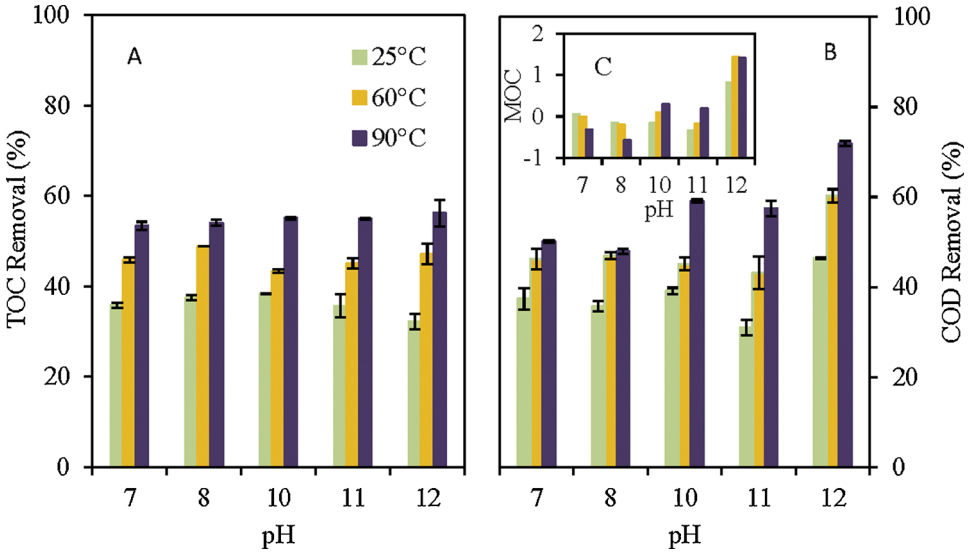

Fig. 8. Removal rates of TOC (A) and COD (B) and MOC of the solution (C) after 3 h of reaction between HS and NCO at different initial pH and temperature.

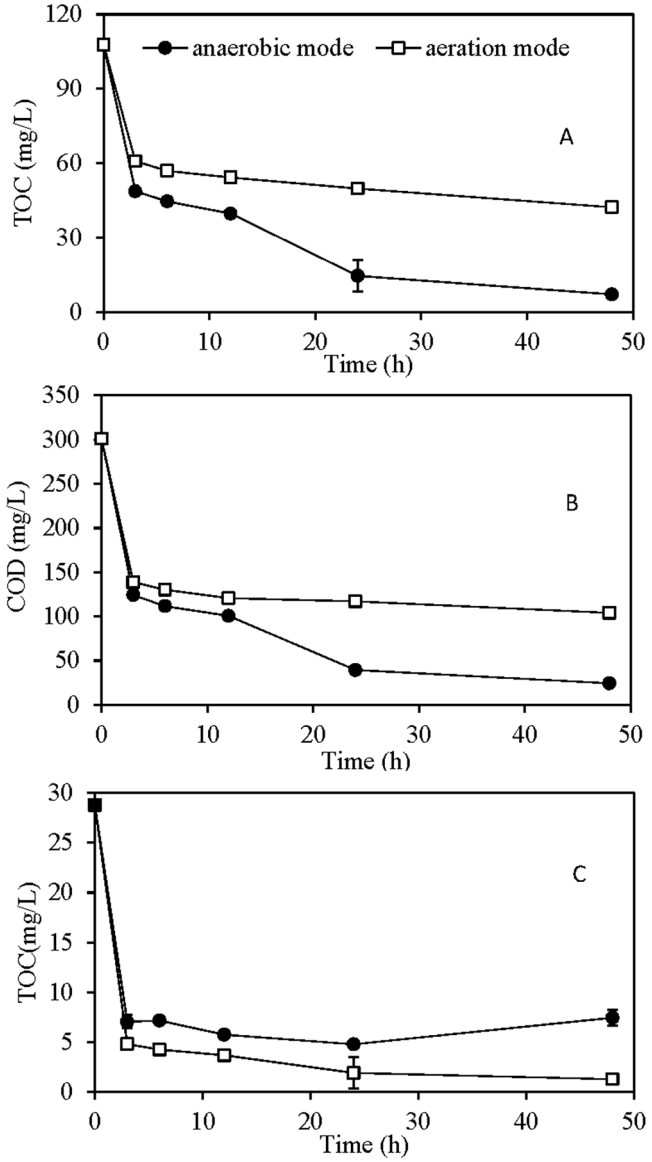

Fig. 9. Variation of TOC and COD in CWAO of anaerobic mode and aeration mode at 90 °C and initial pH 10 (A and B had TOC_0 of 107.8 mg/L; while C had TOC_0 of 28.8 mg/L).

showed that the used NCO had the same pattern with cubic spinel NCO in either anaerobic or aeration mode, verifying that the crystal structure of NCO was robust. Further investigation showed that the SSA of NCO decreased due to the coverage by organic matter. The SSA of NCO in aeration mode was slightly larger than that in anaerobic mode, and the average pore diameter of NCO in aeration mode was also higher than that under anaerobic conditions (Table S1), indicating that aeration promoted the oxidation of organic matter and reduced the accumulation of organic matter on the NCO surface. In addition, the leaching ratios of Ni and Co from NCO were 0.07% and 0.03% for the group with a TOC_0 of 28.8 mg/L, respectively, after 24 h of aeration reaction; for the group with a TOC_0 of 107.8 mg/L, the ratios were 0.33% and 0.06%, respectively. The low metal leaching demonstrated the durability of NCO. Nevertheless, the situation can be further improved by several methods, such as loading NCO on some supports and improving aeration and reactor configuration.

3.2.4. HS degradation process during CWAO with NCO as catalyst

In the aeration group at 90 °C, the solution was diluted 250 times using ultrapure water and then subjected to measurement using MALDI-TOF-MS (Fig. 10). The peaks blow *m/z* 400 and in the range *m/z* 650–750 should be attributed to the DHBA matrices or contaminants [52], and hence the spectra of *m/z* 400–650 and 750–2000 are shown in Fig. 9. The peaks with signal-to-noise ratios higher than 20 were considered for interpretation. Significant peaks appear at *m/z* 1209.3, 1281.8, and 1354.7. Peaks at *m/z* 883, 996.9, 1147.8, 1281.3, and 1564 were previously reported [52], and the difference in *m/z* value of 0.5–2 Da between this work and the literature could be attributed to instrumental errors. A gap of 18 Da existed between peaks, which can be attributed to H_2O [73], and another gap of 73 Da could be attributed to amino-sugar groups [73]. On the whole, more obvious peaks occurred below *m/z* 1000 compared to the spectra of a raw HS solution, indicating the decomposition of the HS into small molecules.

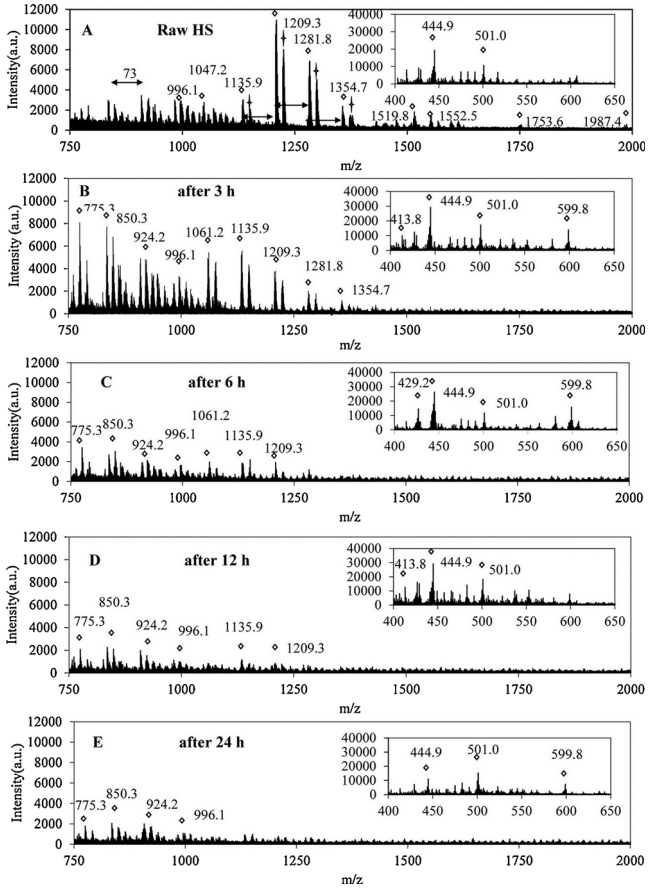

Fig. 10. Mass spectra of raw HS (A) and its intermediates after 3 h (B), 6 h (C), 12 h (D), and 24 h (E) of CWAO using NCO as catalyst at 90 °C.

Fig. S5 shows the GC-MS spectrum of the intermediate products, mainly including 2,4-2 *t*-butylphenol (28.03 min), benzyl benzoate (35.46 min), methyl palmitate (39.51 min), dibutyl phthalate (40.15 min), methyl octadecanoate (44.24 min), and glyceryl 2-hexadecanoate (52.24 min). Similar intermediates had also been found during HS oxidation in a previous study [74]. Combined with the results MALDI-TOF and volatile fatty acid analysis plotted in Fig. S6, it can be concluded that the HS first underwent chemical bond cleavage in the CWAO system through redox, macromolecules were converted into small molecules, and polyphenylene rings were converted into monophenyl rings. Some micromolecular organics, such as carboxylic acids, were eventually completely mineralized into carbonates.

3.3. Catalytic mechanism of NCO during CWAO of HS

To understand the function of NCO during CWAO of HS, XPS measurements were applied to investigate the change of the valence

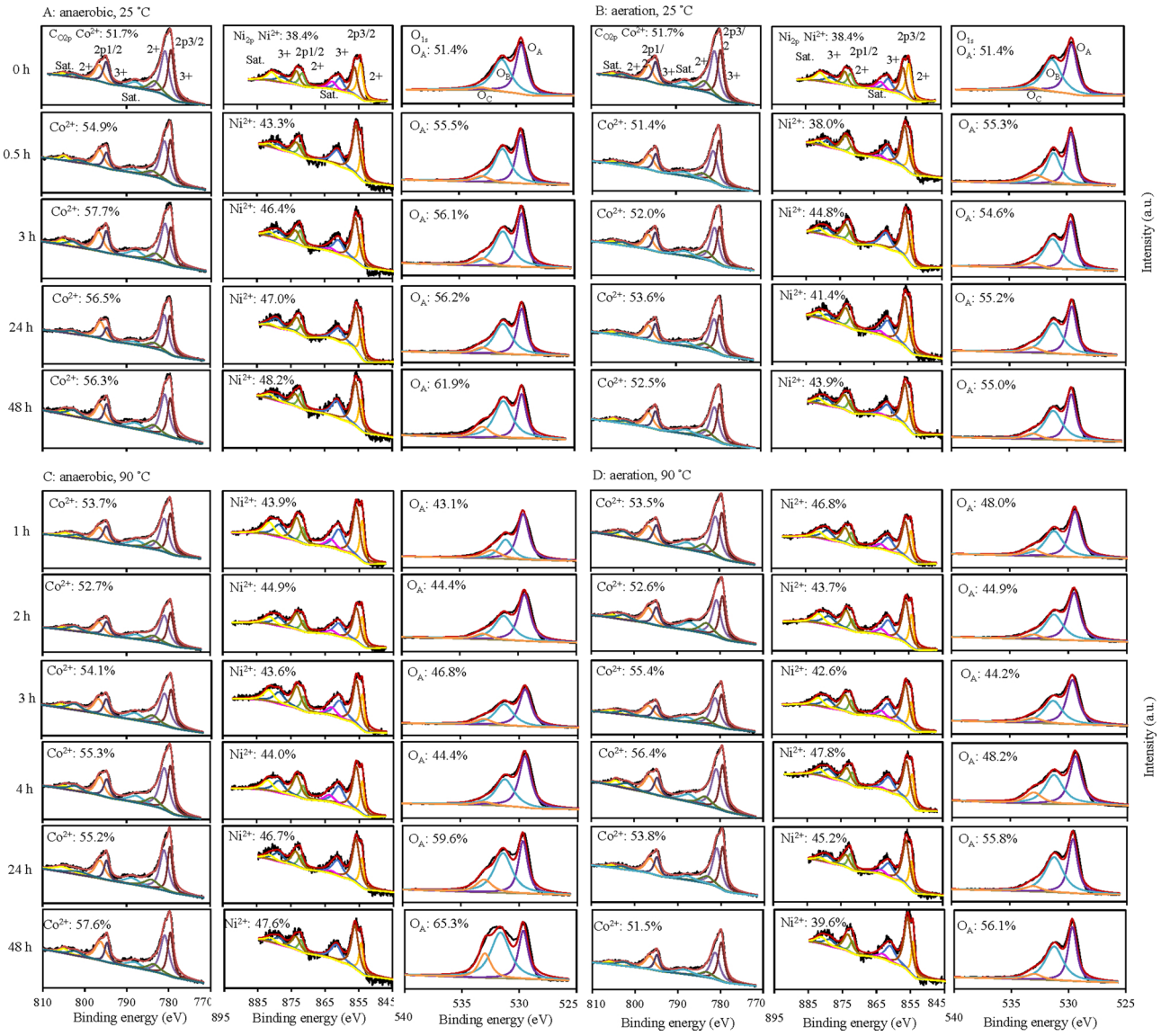

Fig. 11. XPS profiles of NCO under different reaction conditions (A, anaerobic mode at 25 °C; B, aeration mode at 25 °C; C, anaerobic mode at 90 °C; D, aeration mode at 90 °C; the percentages in subfigures indicate the molar ratios of Co^{2+} to Co element, Ni^{2+} to Ni element, and O_A to $O_A + O_B$, respectively).

state of Ni, Co, and O at 25 °C or 90 °C in anaerobic or aeration mode with a TOC_0 of 28.8 mg/L (Fig. 11). At 90 °C in anaerobic mode, the proportions of Ni(II) and Co(II) species rose from 38.4% to 47.6% and from 51.7% to 57.6%, respectively; similarly, at 25 °C, the trends were from 38.4% to 48.2% and from 51.7% to 56.3%, respectively. This illustrates that Ni(III) and Co(III) species worked as oxidants and oxidized HS absorbed on the NCO surface, and high temperature can increase the reactivity of Ni(III) and Co(III) species and accelerate the reaction rate. At 90 °C with oxygen supply, the proportions of Ni(II) increased from 38.4% to 46.8% and then decreased to 39.6%. Similarly, the proportions of Co(II) increased from 51.7% to 56.3% and then decreased to 51.5%. The elemental valence of NCO after 48 h of CWAO was close to that of fresh NCO, verifying that O_2 oxidized Ni(II) and Co (II). For oxygen species, the ratio of OB/(OA + OB) decreased from 51.4% to 43.1% and then increased to 65.3% at 90 °C in anaerobic mode, while the ratio increased from 51.4% to 61.9% at 25 °C. This shows that low temperature was more favorable for the formation of surface hydroxyl groups as they occurred at Lewis sites, but low temperature should be not conducive to the activity of surface hydroxyl groups. The ratio of OB/(OA + OB) had similar trends in the two modes at the same temperature, but the variation was larger in the anaerobic mode because lattice oxygen species converted to surface oxygen for the redox reaction.

At 90 °C with aeration, the valence states of nickel and cobalt indicated that oxygen re-oxidized NCO to its initial state. In addition, the turning point of the change in the ratio of Co(II) occurred later than that of Ni(II), indicating that electron transfer also existed between Ni(III) and Co(II). This change was in line with the electron- and oxygen-transfer reaction mechanisms (denoted ET-OT) of the (MVK mechanism [64,65,75,76]. Thus, in the reaction process, it can be assumed that 1) $\equiv Ni(III) - OH^-$ and $\equiv Co(III) - OH^-$ are formed due to metal ions acting as Lewis sites and combining with H_2O; 2) the HS is adsorbed on the NCO surface by electrostatic adsorption and chemisorption; 3) the hydroxyls formed in the first step, i.e., activated oxygen species [21,56], oxidized the HS directly and resulted in decreased surface oxygen species; 4) the lattice oxygen transformed into surface oxygen species to maintain the balance of the charge on the NCO surface, forming oxygen vacancies; and 4) external O_2 filled the oxygen vacancies and transferred electrons to the reduced catalyst. In anaerobic mode, only the first three steps took place since no oxygen was supplied. Moreover, the catalyst dose was excessive in this study, and the lack of oxygen supply did not limit HS degradation.

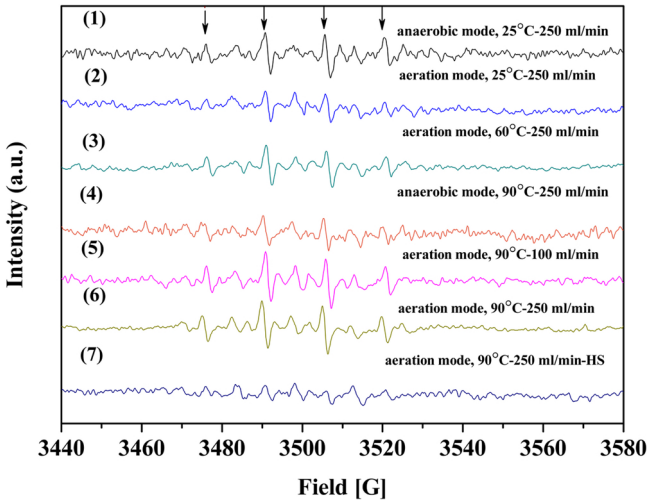

Fig. 12. ESR spectra of DMPO-·OH samples obtained when reactions continued for 20 min (the arrows indicate the characteristic peaks of DMPO-·OH).

In addition to the surface reactions on NCO, free radicals could also contribute to the decomposition of HS. The DMPO-·OH adducts were probed by ESR under different conditions (Fig. 12). Except for the bottom curve with HS addition, the characteristic peaks of DMPO-·OH can be found in other curves, indicating that HS acted as a quencher of ·OH. Referring to the ORR mechanism, H_2O_2, ·OH, $\cdot O_2^-$,$\cdot HO_2^-$, etc. would be generated while the oxygen species absorbed on active sites of NCO are reduced to H_2O while being produced [77,78]. In aeration mode, the concentration of ·OH at 90 °C was higher than that at 25 °C. After 20 min of reaction at 90 °C, the concentration of ·OH in aerobic mode was higher than that in anaerobic mode, while at 25 °C, the concentration of ·OH in anaerobic mode was higher. Hence, the generation of ·OH was influenced by reaction temperature and oxygen concentration that determined the quantity of oxygen species adsorbed on the NCO surface. Thus, free radical reaction also played a role in the oxidation of HS during this CWAO process, and optimized aeration conditions would benefit the generation of ·OH and the HS degradation.

The above results confirm that the synthesized NCO itself can decompose and even mineralize HS, and catalyze oxidative degradation of HS during CWAO. In addition, OH^- and high temperature can enhance the performance. At 90 °C with pH 10, the removal rate of TOC reached 87.2% after 12 h. In fact, NCO could catalyze O_2 to mineralize 75% of the HS in 10 min (the results are not shown). In previous studies, Trellu et al. [19] achieved mineralization of HS solution with a TOC_0 of 16.2 mg/L after 7 h of anodic oxidation treatment using boron-doped diamond anode, a stainless-steel cathode, and a current intensity of 1 A. Yao et al. [49] used H_2O_2 as the oxidant and CuO-Co_3O_4 as the catalyst to degrade a 100-mg/L HS under microwave irradiation, and the removal efficiency of the HS and TOC reached 88% and 71%, respectively. Tian et al. [79] used dandelion-like $NiCo_2O_4$ microspheres to activate peroxymonosulfate in HS degradation, and the HS removal rate exceeded 90% within 2 h. Compared with these works, in this study a high mineralization rate of HS was achieved at atmospheric pressure and without using chemicals. This implies that the proposed method employed with a particular NCO should be an inexpensive and easy way to solve the problem of wastewater containing HS.

4. Conclusions

Microspheres constituted of $NiCo_2O_4$ spinel were synthesized that had high oxidative activity to HS owing to its unique hierarchical architectures, the synergistic effect of redox pairs, and high activity of surface oxygen. The CWAO process using NCO as the catalyst followed the MVK mechanism, i.e., ≡Co(III), ≡Ni(III), and all the oxygen species participated in the HS degradation. In addition, some O_2 absorbed on NCO surface turned into ·OH, which facilitated the HS degradation. With the help of NCO, the removal rate of TOC exceeded 90% during CWAO at atmospheric pressure and 90 °C in 24 h. High pH and high temperature can enhance the performance of NCO. This study provides a possible new way to treat HS-rich water under mild conditions.

Acknowledgement

Financial support for this project is obtained from the National Key R&D Program of China (grant number 2018YFC1902900); the Shenzhen Science and Technology Project (grant number JCYJ20170817161931586); and the Development and Reform Commission of Shenzhen Municipality (urban water recycling and environment safety program).

Appendix A. Supplementary data

Supplementary material related to this article can be found, in the online version, at doi:https://doi.org/10.1016/j.apcatb.2019.117858.

References

[1] M. Sillanpaa, M.C. Ncibi, A. Matilainen, Advanced oxidation processes for the removal of natural organic matter from drinking water sources: a comprehensive review, J. Environ. Manage. 208 (2018) 56–76.
[2] H. Katsumata, M. Sada, S. Kaneco, T. Suzuki, K. Ohta, Y. Yobiko, Humic acid degradation in aqueous solution by the photo-Fenton process, Chem. Eng. J. 137 (2008) 225–230.
[3] Y. Yang, H. Li, J. Li, Variation in humic and fulvic acids during thermal sludge treatment assessed by size fractionation, elementary analysis, and spectroscopic methods, Front. Environ. Sci. Eng. 8 (2014) 854–862.
[4] H. Li, Y. Li, C. Li, Evolution of humic substances during anaerobic sludge digestion, Environ. Eng. Manage. J. 16 (2017) 1577–1582.
[5] Y. Yang, H. Li, Recovering humic substances from the dewatering effluent of thermally treated sludge and its performance as an organic fertilizer, Front. Environ. Sci. Eng. 10 (2015) 578–584.
[6] T. Bond, M.R. Templeton, O. Rifai, H. Ali, N.J.D. Graham, Chlorinated and nitrogenous disinfection by-product formation from ozonation and post-chlorination of natural organic matter surrogates, Chemosphere 111 (2014) 218–224.
[7] H. Li, Y. Li, C. Li, Characterization of humic acids and fulvic acids derived from sewage sludge, Asian J. Chem. 25 (2013) 10087–10091.
[8] C.E.W. Steinberg, Humic substances in the environment with an emphasis on freshwater systems, Environ. Sci. Pollut. Res. - Int. 15 (2008) 15–16.
[9] T.V. Fernandes, J.B.V. Lier, G. Zeeman, Humic acid-like and fulvic acid-like inhibition on the hydrolysis of cellulose and tributyrin, Bioenergy Res. 8 (2015) 821–831.
[10] E. Mohora, S. Rončević, B. Dalmacija, J. Agbaba, M. Watson, E. Karlović, M. Dalmacija, Removal of natural organic matter and arsenic from water by electrocoagulation/flotation continuous flow reactor, J. Hazard. Mater. 235–236 (2012) 257–264.
[11] K. Torbjörn, P. Per, S. Ulf, Extended X-ray absorption fine structure spectroscopy evidence for the complexation of cadmium by reduced sulfur groups in natural organic matter, Environ. Sci. Technol. 39 (2005) 3048–3055.
[12] B.M. Wilen, B. Jin, P. Lant, The influence of key chemical constituents in activated sludge on surface and flocculating properties, Water Res. 37 (2003) 2127–2139.
[13] R.L. Cook, C.H. Langford, Structural characterization of a fulvic acid and a humic acid using solid-state Ramp-CP-MAS ^{13}C nuclear magnetic resonance, Environ. Sci. Technol. 32 (2009) 719–725.
[14] A. Matilainen, M. Vepsäläinen, M. Sillanpää, Natural organic matter removal by coagulation during drinking water treatment: a review, Adv. Colloid Interface Sci. 159 (2010) 189–197.
[15] S. Mozia, M. Tomaszewska, A.W. Morawski, Studies on the effect of humic acids and phenol on adsorption-ultrafiltration process performance, Water Res. 39 (2005) 501–509.
[16] S.G.J. Heijman, A.M.V. Paassen, W.G.J.V.D. Meer, R. Hopman, Adsorptive removal of natural organic matter during drinking water treatment, Water Sci. Technol. 40 (1999) 183–190.
[17] S. Cortez, P. Teixeira, R. Oliveira, M. Mota, Ozonation as polishing treatment of mature landfill leachate, J. Hazard. Mater. 182 (2010) 730–734.
[18] C. Trellu, Y. Péchaud, N. Oturan, E. Mousset, D. Huguenot, E.D. van Hullebusch, G. Esposito, M.A. Oturan, Comparative study on the removal of humic acids from drinking water by anodic oxidation and electro-Fenton processes: mineralization efficiency and modelling, Appl. Catal. B 194 (2016) 32–41.
[19] S. Ye, M. Yan, X. Tan, J. Liang, G. Zeng, H. Wu, B. Song, C. Zhou, Y. Yang, H. Wang, Facile assembled biochar-based nanocomposite with improved graphitization for efficient photocatalytic activity driven by visible light, Appl. Catal. B 250 (2019) 78–88.
[20] Y. Ren, L. Lin, J. Ma, Y. Jing, F. Jing, Z. Fan, Sulfate radicals induced from peroxymonosulfate by magnetic ferrospinel MFe_2O_4 (M = Co, Cu, Mn, and Zn) as heterogeneous catalysts in the water, Appl. Catal. B 165 (2015) 572–578.
[21] Y. Yao, Y. Cai, G. Wu, F. Wei, X. Li, H. Chen, S. Wang, Sulfate radicals induced from

peroxymonosulfate by cobalt manganese oxides ($Co_xMn_{3-x}O_4$) for Fenton-Like reaction in water, J. Hazard. Mater. 296 (2015) 128–137.
[22] M. Čehovin, A. Medic, J. Scheideler, J. Mielcke, A. Ried, B. Kompare, A.Ž. Gotvajn, Hydrodynamic cavitation in combination with the ozone, hydrogen peroxide and the UV-based advanced oxidation processes for the removal of natural organic matter from drinking water, Ultrason. Sonochem. 37 (2017) 394–404.
[23] K.H. Kim, S.K. Ihm, Heterogeneous catalytic wet air oxidation of refractory organic pollutants in industrial wastewaters: a review, J. Hazard. Mater. 186 (2011) 16–34.
[24] W.M. Liu, Y.Q. Hu, S.T. Tu, Active carbon–ceramic sphere as support of ruthenium catalysts for catalytic wet air oxidation (CWAO) of resin effluent, J. Hazard. Mater. 179 (2010) 545–551.
[25] W. Cao, H. Chen, Y. Feng, C. Shi, S. Xu, G. Yang, X. Zhang, Biodegradability enhancement of coking wastewater by catalytic wet air oxidation using aminated activated carbon as catalyst, Chem. Eng. J. 198–199 (2012) 45–51.
[26] R.J.G. Lopes, T.S.A. Almeida, R.M. Quinta-Ferreira, Integrated detoxification methodology of hazardous phenolic wastewaters in environmentally based trickle-bed reactors: experimental investigation and CFD simulation, J. Hazard. Mater. 189 (2011) 108–118.
[27] S.D. Yim, J.K. Dong, I.S. Nam, A pilot plant study for catalytic decomposition of PCDDs/PCDFs over supported chromium oxide catalysts, Catal. Today 75 (2002) 269–276.
[28] E.E. Iojoiu, E. Landrivon, H. Raeder, E.G. Torp, S. Miachon, J.A. Dalmon, The "Watercatox" process: wet air oxidation of industrial effluents in a catalytic membrane reactor: first report on contactor CMR up-scaling to pilot unit, Catal. Today 118 (2006) 246–252.
[29] A. Singh, K.K. Pant, K.D.P. Nigam, Catalytic wet oxidation of phenol in a trickle bed reactor, Chem. Eng. J. 103 (2004) 51–57.
[30] Z.L. Arsenijevic, B.V. Grbic, N.D. Radic, L.B. Grbavcic, Catalytic incineration of ethylene oxide in the packed bed reactor, Chem. Eng. J. 116 (2006) 173–178.
[31] H. Delmas, C. Creanga, C. Julcour-Lebigue, A.M. Wilhelm, AD–OX: a sequential oxidative process for water treatment—adsorption and batch CWAO regeneration of activated carbon, Chem. Eng. J. 152 (2009) 189–194.
[32] R.J.G. Lopes, R.M. Quinta-Ferreira, Assessment of CFD Euler–Euler method for trickle-bed reactor modelling in the catalytic wet oxidation of phenolic wastewaters, Chem. Eng. J. 160 (2010) 293–301.
[33] Q. Wu, X. Hu, P.L. Yue, J. Feng, X. Chen, H. Zhang, S. Qiao, Modeling of a pilot-scale trickle bed reactor for the catalytic oxidation of phenol, Sep. Purif. Technol. 67 (2009) 158–165.
[34] Y. Xu, D. Sun, Structure and catalytic activity of Mo-Zn-Al-O catalyst for degradation of cationic red GTL under room conditions, Chem. Eng. J. 183 (2012) 332–338.
[35] Y. Xu, X. Li, X. Cheng, D. Sun, X. Wang, Degradation of cationic red GTL by catalytic wet air oxidation over Mo–Zn–Al–O catalyst under room temperature and atmospheric pressure, Environ. Sci. Technol. 46 (2012) 2856–2863.
[36] S. Zhao, X. Wang, M. Huo, Catalytic wet air oxidation of phenol with air and micellar molybdovanadophosphoric polyoxometalates under room condition, Appl. Catal. B 97 (2010) 127–134.
[37] P. Oulego, S. Collado, A. Laca, M. Diaz, Impact of leachate composition on the advanced oxidation treatment, Water Res. 88 (2016) 389–402.
[38] A. Anglada, A. Urtiaga, I. Ortiz, D. Mantzavinos, E. Diamadopoulos, Treatment of municipal landfill leachate by catalytic wet air oxidation: assessment of the role of operating parameters by factorial design, Waste Manag. 31 (2011) 1833–1840.
[39] X.-Y. Xu, G.-M. Zeng, Y.-R. Peng, Z. Zeng, Potassium persulfate promoted catalytic wet oxidation of fulvic acid as a model organic compound in landfill leachate with activated carbon, Chem. Eng. J. 200–202 (2012) 25–31.
[40] P. Wang, G. Zeng, Y. Peng, F. Liu, C. Zhang, B. Huang, Y. Zhong, Y. He, M. Lai, 2,4,6-Trichlorophenol-promoted catalytic wet oxidation of humic substances and stabilized landfill leachate, Chem. Eng. J. 247 (2014) 216–222.
[41] G.R. Peterson, H.L. Fernando, G. Cenk, W.P. Bassett, K. Carol, L.J. Hope-Weeks, Preparation-morphology-performance relationships in cobalt aerogels as supercapacitors, ACS Appl. Mater. Interfaces 6 (2014) 1796–1803.
[42] R. Ding, L. Qi, M. Jia, H. Wang, Facile synthesis of mesoporous spinel $NiCo_2O_4$ nanostructures as highly efficient electrocatalysts for urea electro-oxidation, Nanoscale 6 (2014) 1369–1376.
[43] X.Y. Yu, X.Z. Yao, T. Luo, Y. Jia, J.H. Liu, X.J. Huang, Facile synthesis of urchin-like $NiCo_2O_4$ hollow microspheres with enhanced electrochemical properties in energy and environmentally related applications, ACS Appl. Mater. Interfaces 6 (2014) 3689–3695.
[44] Q. Zhao, Z. Yan, C. Chen, J. Chen, Spinels: controlled preparation, oxygen Reduction/Evolution reaction application, and beyond, Chem. Rev. 117 (2017) 10121–10211.
[45] X. Tian, T. Chen, Y. Nie, D. Chu, Y. Chao, T. Na, Z. Zhou, L. Yong, Y. Wang, Controlled synthesis of dandelion-like $NiCo_2O_4$ microspheres and their catalytic performance for peroxymonosulfate activation in humic acid degradation, Chem. Eng. J. (2017) S1385894717314560.
[46] W. Zhang, Y. Su, X. Zhang, Y. Yang, X. Guo, Facile synthesis of porous $NiCo_2O_4$ nanoflakes as magnetic recoverable catalysts towards the efficient degradation of RhB, RSC Adv. 6 (2016) 64626–64633.
[47] X. Liu, D. Xu, D. Zhang, G. Zhang, L. Zhang, Superior performance of 3 D Co-Ni bimetallic oxides for catalytic degradation of organic dye: investigation on the effect of catalyst morphology and catalytic mechanism, Appl. Catal. B 186 (2016) 193–203.
[48] J. Deng, S. Feng, K. Zhang, J. Li, H. Wang, T. Zhang, X. Ma, Heterogeneous activation of peroxymonosulfate using ordered mesoporous Co_3O_4 for the degradation of chloramphenicol at neutral pH, Chem. Eng. J. 308 (2017) 505–515.
[49] X. Yao, Q. Lin, L. Zeng, J. Xiang, G. Yin, Q. Liu, Degradation of humic acid using hydrogen peroxide activated by CuO-Co_3O_4@AC under microwave irradiation, Chem. Eng. J. 330 (2017) 783–791.
[50] C. Jin, F. Lu, X. Cao, Z. Yang, R. Yang, Facile synthesis and excellent electrochemical properties of $NiCo_2O_4$ spinel nanowire arrays as a bifunctional catalyst for the oxygen reduction and evolution reaction, J. Mater. Chem. A 1 (2013) 12170.
[51] Ministry of Environmental Protection, Standard Methods for the Examination, f.e.M. of Water and Wastewater, Beijing, China., C.M, 2002.
[52] S.M. Mugo, C.S. Bottaro, Characterization of humic substances by matrix-assisted laser desorption/ionization time-of-flight mass spectrometry, Rapid Communications in Mass Spectrometry Rcm 18 (2004) 2375–2382.
[53] W. Zhang, X. Di, L. Xue, W. Ye, X. Jiang, Y. Wang, W. Liang, Electrocatalytic removal of humic acid using cobalt-modified particle electrodes, Appl. Catal. A Gen. 559 (2018) 75–84.
[54] C. Zhang, X. Geng, S. Tang, M. Deng, Y. Du, $NiCo_2O_4$@rGO hybrid nanostructures on Ni foam as high-performance supercapacitor electrodes, J. Mater. Chem. A 5 (2017) 5912–5919.
[55] L. Gu, L. Qian, Y. Lei, Y. Wang, J. Li, H. Yuan, D. Xiao, Microwave-assisted synthesis of nanosphere-like $NiCo_2O_4$ consisting of porous nanosheets and its application in electro-catalytic oxidation of methanol, J. Power Sources 261 (2014) 317–323.
[56] Y. Yao, Y. Cai, G. Wu, F. Wei, X. Li, C. Hao, S. Wang, Sulfate radicals induced from peroxymonosulfate by cobalt manganese oxides ($Co_xMn_{3-x}O_4$) for Fenton-Like reaction in water, J. Hazard. Mater. 296 (2015) 128–137.
[57] M.R. Benzigar, S.N. Talapaneni, S. Joseph, K. Ramadass, G. Singh, J. Scaranto, U. Ravon, K. Al-Bahily, A. Vinu, Recent advances in functionalized micro and mesoporous carbon materials: synthesis and applications, Chem. Soc. Rev. 47 (2018) 2680–2721.
[58] W. Yuan, H. Arandiyan, J. Scott, A. Bagheri, H. Dai, R. Amal, Recent advances in ordered meso/macroporous metal oxides for heterogeneous catalysis: a review, J. Mater. Chem. A 5 (2017).
[59] A. Galtayries, R. Sporken, J. Riga, G. Blanchard, R. Caudano, XPS comparative study of ceria/zirconia mixed oxides: powders and thin film characterisation, J. Electron Spectros. Relat. Phenomena 88–91 (1998) 951–956.
[60] H. Chen, A. Sayari, A. Adnot, F.Ç. Larachi, Composition–activity effects of Mn–Ce–O composites on phenol catalytic wet oxidation, Appl. Catal. B 32 (2001) 195–204.
[61] F. Larachi, J. Pierre, A. Adnot, A. Bernis, Ce 3d XPS study of composite $Ce_xMn_{1-x}O_{2-y}$ wet oxidation catalysts, Appl. Surf. Sci. 195 (2002) 236–250.
[62] S. Hosokawa, H. Kanai, K. Utani, Y.I. Taniguchi, Y. Saito, S. Imamura, State of Ru on CeO and its catalytic activity in the wet oxidation of acetic acid, Appl. Catal. B 45 (2003) 181–187.
[63] J.B Jr, F. Delanoë, F. Jabouille, D. Duprez, G. Blanchard, P. Isnard, Total oxidation of acetic acid in aqueous solutions over noble metal catalysts, J. Catal. 177 (1998) 378–385.
[64] S.K. Bhargava, J. Tardio, J. Prasad, K. Foger, D.B. Akolekar, S.C. Groccott, Wet oxidation and catalytic wet oxidation, Ind. Eng. Chem. Res. 45 (2006) 1221–1258.
[65] Gl. Ersöz, Sh. Atalay, Kinetic modeling of the removal of aniline by low-pressure catalytic wet air oxidation over a nanostructured Co_3O_4/CeO_2 catalyst, Ind. Eng. Chem. Res. 50 (2015) 310–315.
[66] Y. Lou, L. Wang, Z. Zhao, Y. Zhang, Z. Zhang, G. Lu, Y. Guo, Y. Guo, Low-temperature CO oxidation over Co_3O_4-based catalysts: significant promoting effect of Bi_2O_3 on Co_3O_4 catalyst, Appl. Catal. B 146 (2014) 43–49.
[67] X. Wang, W. Wen, J. Mi, X. Li, R. Wang, The ordered mesoporous transition metal oxides for selective catalytic reduction of NOx at low temperature, Appl. Catal. B 176 (2015) 454–463.
[68] X. Wang, W. Zhao, X. Wu, T. Zhang, L. Yi, Z. Kai, Y. Xiao, L. Jiang, X. Wang, W. Zhao, Total oxidation of benzene over ACo_2O_4 (A = Cu, Ni and Mn) catalysts: in situ DRIFTS account for understanding the reaction mechanism, Appl. Surf. Sci. 426 (2017) S0169433217322699.
[69] S. Zhang, X. Zhu, C. Zheng, D. Hu, J. Zhang, X. Gao, Study on catalytic soot oxidation over spinel type ACo_2O_4 (A = Co, Ni, Cu, Zn) catalysts, Aerosol Air Qual. Res. 17 (2017) 2317–2327.
[70] A.B.M. Giasuddin, S.R. Kanel, C. Heechul, Adsorption of humic acid onto nanoscale zerovalent iron and its effect on arsenic removal, Environ. Sci. Technol. 41 (2007) 2022–2027.
[71] F. Vogel, J. Harf, A. Hug, P.R.V. Rohr, The mean oxidation number of carbon (MOC)—a useful concept for describing oxidation processes, Water Res. 34 (2000) 2689–2702.
[72] B.R. Yadav, A. Garg, Catalytic wet oxidation of ferulic acid (a lignin model compound) in the presence of non-noble metal based catalysts at mild conditions, Chem. Eng. J. 252 (2014) 185–193.
[73] G. Plancque, B. Amekraz, V. Moulin, P. Toulhoat, C. Moulin, Molecular structure of fulvic acids by electrospray with quadrupole time-of-flight mass spectrometry, Rapid Communications in Mass Spectrometry Rcm 15 (2010) 827–835.
[74] S.D. Killops, Volatile ozonization products of aqueous humic material, Water Res. 20 (1986) 153–165.
[75] A.M. Khenkin, L. Weiner, Y. Wang, R. Neumann, Electron and oxygen transfer in polyoxometalate, $H_5PV_2Mo_{10}O_{40}$, catalyzed oxidation of aromatic and alkyl aromatic compounds: evidence for aerobic Mars-van Krevelen-type reactions in the liquid homogeneous phase, J. Am. Chem. Soc. 123 (2001) 8531–8542.
[76] A.M. Khenkin, N. Ronny, Oxidative C-C bond cleavage of primary alcohols and vicinal diols catalyzed by $H_5PV_2Mo_{10}O_{40}$ by an electron transfer and oxygen transfer reaction mechanism, J. Am. Chem. Soc. 130 (2008) 14474–14476.
[77] H. Zhao, C. Ying, Q. Peng, Q. Wang, G. Zhao, Catalytic activity of MOF(2Fe/Co)/carbon aerogel for improving H_2O_2 and ·OH generation in solar photo–electro–Fenton process, Appl. Catal. B 203 (2017) 127–137.
[78] N.L. Jean-Marc, L. Alina, L. Corinne, V. Elena, H. Philippe, Evidence for ·OH radical production during electrocatalysis of oxygen reduction on Pt surfaces: consequences and application, J. Am. Chem. Soc. 134 (2012) 2835–2841.
[79] X. Tian, C. Tian, Y. Nie, C. Dai, C. Yang, N. Tian, Z. Zhou, Y. Li, Y. Wang, Controlled synthesis of dandelion-like $NiCo_2O_4$ microspheres and their catalytic performance for peroxymonosulfate activation in humic acid degradation, Chem. Eng. J. 331 (2018) 144–151.